The Cryosphere, 6, 35–50, 2012
www.the-cryosphere.net/6/35/2012/
doi:10.5194/tc-6-35-2012

The Cryosphere

The impact of a seasonally ice free Arctic Ocean on the temperature, precipitation and surface mass balance of Svalbard

J. J. Day[1,2], **J. L. Bamber**[1], **P. J. Valdes**[1], **and J. Kohler**[3]

[1]School of Geographical Sciences, University of Bristol, Bristol, UK
[2]RIGC/JAMSTEC, Yokohama Institute for Earth Sciences, Yokohama, Japan
[3]Norsk Polarinstitutt, Polar Environment Centre, Tromsø, Norway

Correspondence to: J. J. Day (jday@jamstec.go.jp)

Received: 24 June 2011 – Published in The Cryosphere Discuss.: 18 July 2011
Revised: 4 December 2011 – Accepted: 17 December 2011 – Published: 10 January 2012

Abstract. The observed decline in summer sea ice extent since the 1970s is predicted to continue until the Arctic Ocean is seasonally ice free during the 21st Century. This will lead to a much perturbed Arctic climate with large changes in ocean surface energy flux. Svalbard, located on the present day sea ice edge, contains many low lying ice caps and glaciers and is expected to experience rapid warming over the 21st Century. The total sea level rise if all the land ice on Svalbard were to melt completely is 0.02 m.

The purpose of this study is to quantify the impact of climate change on Svalbard's surface mass balance (SMB) and to determine, in particular, what proportion of the projected changes in precipitation and SMB are a result of changes to the Arctic sea ice cover. To investigate this a regional climate model was forced with monthly mean climatologies of sea surface temperature (SST) and sea ice concentration for the periods 1961–1990 and 2061–2090 under two emission scenarios. In a novel forcing experiment, 20th Century SSTs and 21st Century sea ice were used to force one simulation to investigate the role of sea ice forcing. This experiment results in a 3.5 m water equivalent increase in Svalbard's SMB compared to the present day. This is because over 50 % of the projected increase in winter precipitation over Svalbard under the A1B emissions scenario is due to an increase in lower atmosphere moisture content associated with evaporation from the ice free ocean. These results indicate that increases in precipitation due to sea ice decline may act to moderate mass loss from Svalbard's glaciers due to future Arctic warming.

1 Introduction

Worldwide, observations of glaciers show an increasingly negative mass balance in recent years (Arendt et al., 2002; Kaser et al., 2006). Despite the fact that only 0.5 % of the Earth's terrestrial cryosphere consists of small glaciers and ice caps outside the ice sheets (Antarctica and Greenland), the smaller ice masses in the Arctic are thought to be a major contribution to this negative balance (Meier et al., 2007). The mean annual contribution from the Arctic is estimated to have increased from 0.27 mm a^{-1} sea level equivalent (SLE) between 1961–1992 to 0.64 mm a^{-1} between 1993–2006 (Dyurgerov et al., 2010). Svalbard contributes to this total, with estimates ranging from 0.013 to 0.026 mm a^{-1} SLE (Moholdt et al., 2010; Nuth et al., 2010; Wouters et al., 2008). Svalbard contains an estimated 7000 km^3 of ice and were this to melt completely it would cause 0.02 m of eustatic sea level rise (Hagen et al., 2003).

Sea ice extent around Svalbard has been decreasing since the mid-1800s (Divine and Dick, 2006), concurrent with a general increase in temperatures (Nordli and Kohler, 2004). This sector contributes to the negative trend in total Arctic sea ice extent, which has accelerated since the 1990s (Overland and Wang, 2007; Serreze et al., 2007). Arctic sea ice retreat is thought to be a major cause of the positive trend in lower tropospheric Arctic temperature, which is amplified with respect to the global mean (Serreze et al., 2009). This decline in sea ice and the associated amplified temperature trend is expected to continue until the Arctic is seasonally ice-free at some point in the 21st Century (Boé et al., 2009; Wang and Overland, 2009).

There is substantial evidence that Svalbard's climate is strongly influenced by variability in the local sea ice edge

Fig. 1. Map of the Svalbard archipelago including names of islands (Large font), locations discussed in this study (bold) and major ice caps (italic).

(Benestad et al., 2002b). Both the West Spitsbergen Current and the leading mode of North Atlantic atmospheric variability, the North Atlantic Oscillation (NAO) are known to be associated with this variability (Yamamoto et al., 2006; Walczowski and Piechura, 2011). Positive NAO years often correspond with low levels of sea ice in the Barents Sea and associated anomalously high precipitation over Svalbard (Rogers et al., 2001). Consequently, it is believed that sea ice variability impacts the surface mass balance (SMB) of glaciers in the region, particularly on Nordaustlandet, which lies at the north-eastern limit of the archipelago (see Fig. 1). Observations suggest that on the Nordaustlandet ice caps: Austfonna and Vestfonna, accumulation is significantly affected by coastal sea ice conditions (Bamber et al., 2004; Möller et al., 2011a). This is because reduced sea ice cover increases the moisture flux from the ocean to the atmosphere, increasing humidity in the region (Raper et al., 2005).

Temperature in Svalbard is also known to be correlated with the position of the sea ice edge. The δ^{18}O record, i.e. temperature in an ice core recovered from the Austfonna ice cap correlates closely to sea ice extent in the region over the last 400 years (Isaksson et al., 2005a,b). However, the correlation between temperature and sea ice extent at the inland, high elevation Lomonosovfonna ice core site is much lower than at Austfonna (Isaksson et al., 2005b). This indicates that proximity to the ocean is an important factor in determining how much local conditions are affected by sea ice variability. The present day sensitivity of Svalbard's climate to local sea ice properties suggests that temperature and precipitation would be greatly affected were the Arctic to become seasonally ice free. Further, the increase in precipitation during low sea ice conditions also suggests sea ice decline will affect SMB by increasing accumulation, particularly in winter. This idea is supported by Singarayer et al. (2006) who suggest that during the 21st Century other areas of Arctic land ice will receive increased accumulation, caused by greater evaporation as Arctic sea ice extent decreases.

It is not possible to test this theory empirically. Neither observations nor proxy reconstructions of SMB exist on Svalbard for past periods when the Arctic Ocean was seasonally ice free. This probably last occurred during the last interglacial at Marine Isotope Stage 5e ∼128 ka BP (Polyak et al., 2010). This predates ice core records on Svalbard, which cover the last 1000 years (Divine et al., 2011a). It is however possible to perform simulations of a seasonally ice free Arctic climate using an atmospheric climate model (e.g. Singarayer et al., 2006; Deser et al., 2010), which is the approach taken in this study. We investigated the impact of a seasonally ice free Arctic Ocean on temperature, precipitation and land ice SMB on Svalbard using a regional climate model (RCM). For this purpose a number of time slice experiments were performed with the RCM. This included two standard IPCC scenarios and one simulation forced by present day sea surface temperatures (SSTs) and late 21st Century sea ice concentration, so that only changes due to sea ice are simulated (e.g Deser et al., 2010; Stein and Alpert, 1993). The modelled temperature and precipitation were used to estimate the change in SMB using the seasonal sensitivity characteristic (SSC) method of Oerlemans et al. (2005).

In a recent study, Førland et al. (2009) used the 25 km NorACIA-RCM version of HIRHAM to simulate 21st Century climate change in Svalbard. They predict that under the special report on emission scenarios (SRES) B2 ("low end") emissions scenario (Nakicenovic and Swart, 2000), Svalbard will experience an annual temperature increase of 3 °C in the south west and 8 °C in the north east from 1961–1990 to 2071–2100 with larger changes in winter than summer. Annual precipitation is expected to increase by 10 % in the south west and 40 % in the north east over the same period (Førland et al., 2009).

In this study, we used a 25 km version of the UK Met Office Hadley Centre (MOHC) RCM, HadRM3, to dynamically downscale output from an Atmospheric General Circulation Model (AGCM) (Jones et al., 1995). At this resolution, the RCM captures the essential topography required to model circulation in the region but does not resolve individual valleys or glaciers, many of which are an order of magnitude smaller than the grid cell width (Liestøl, 1993). Here, we extend the work of Førland et al. (2009) by using two "high end" emissions scenarios and incorporating an explicit investigation of the relative importance of sea ice decline on Svalbard's future climate and SMB. The paper is set out as follows: in Sect. 2, we describe the experimental methodology, model setup and validation data. Section 3 describes the validation of model temperature an precipitation. The changes

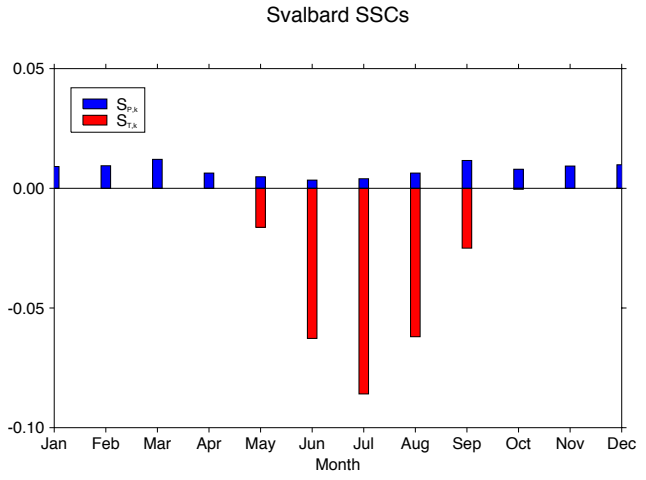

Fig. 2. Seasonal sensitivity characteristics (SSCs) for Svalbard reproduced from Oerlemans et al. (2005). These were averaged from the SSCs of a number of glaciers in Svalbard.

in climate and SMB between the sea ice free scenarios and the present day climate are discussed in Sect. 4, followed by the conclusions.

2 Methodology and model description

2.1 Methodology

Due to Svalbard's relatively small size, downscaling of General Circulation Model (GCM) simulations is required to create climate projections for the archipelago (e.g. Hanssen-Bauer and Førland, 2001). RCMs are commonly used to dynamically downscale GCM projections (e.g. Christensen et al., 2007). They are able to add information at fine scales due to their increased resolution and ability to resolve circulation associated with small scale orographic features (Feser, 2006). Such models are forced at the surface by SSTs and sea ice but also at the lateral boundary by sea level pressure, wind, temperature and humidity.

Surface forcing for RCM experiments was taken from simulations with the MOHC HadGEM1 GCM. These HadGEM1 simulations are part of the World Climate Research Programme's (WCRP's) Coupled Model Intercomparison Project phase 3 (CMIP3) multi-model dataset (http://www-pcmdi.llnl.gov/ipcc/about_ipcc.php). For the reference simulation, we used a historical run for the 20th Century, for which HadGEM1 was forced with observed greenhouse gas (GHG) concentrations (20C3M). Nakicenovic and Swart (2000) set out scenarios of 21st Century GHG emissions, of these we selected A1B, and A2 which are both high end emission scenarios selected to create a large change in sea ice extent. The A1B and A2 scenarios are similar through the early part of the 21st Century but diverge, with A1B describing higher emissions in the last quarter century. The RCM was used to downscale time slices of these 3 climate scenarios and one novel forcing experiment. The time intervals used to create the surface forcing for the models were as follows:

1. 20C3M: present day control SST and sea ice (1961–1990),
2. A1B: A1B SST and sea ice (2061–2090),
3. A2: A2 SST and sea ice (2061–2090) and
4. HYB: A1B sea ice (2061–2090) and 20C3M SSTs (1961–1990).

Hereafter, these simulations will simply be referred to as 20C3M, A1B, A2 and HYB. To separate changes in precipitation and SMB caused by sea ice decline from those associated with the concurrent increase in SSTs a hybrid forcing was used. In this hybrid simulation, HYB, the RCM is forced with 20C3M SST and A1B sea ice. The HYB SST field is not a priori defined for grid points which are ice covered in the 20C3M sea ice field but not in the A1B field. For this experiment we followed Deser et al. (2010) in setting SST in these grid points to the freezing point of sea water (-1.8 °C). The comparison between the HYB and A1B experiments allowed us to isolate climate signals which are the result of changes in sea ice alone from those which are the combined effect of SST and sea ice change. We then used the changes in precipitation and temperature from these simulations to investigate their impact on SMB. To do this we employed the SSC method (Oerlemans and Reichert, 2000; Oerlemans et al., 2005). In this method the SMB anomaly is calculated as a function of changes to Svalbard's area-averaged monthly mean precipitation and temperature as described in Eq. 2.

For a given glacier, its SSCs form a 2×12 matrix describing the sensitivity of its mean net specific SMB ($\bar{b}_n$) to a changes in temperature and precipitation for all months. The SSCs used in this study are averaged from the SSCs of a number of glaciers in Svalbard as described by Oerlemans et al. (2005), whose data are reproduced in Fig. 2. These were calculated by perturbing the temperature and precipitation inputs to an energy balance model as described in Van de Wal and Oerlemans (1994). The following describes how the SSCs are formally defined. The change in mean specific balance of a glacier surface due to a change in climate, may be expressed as:

$$\Delta\bar{b}_n = \bar{b}_n - \bar{b}_{n,\mathrm{ref}}, \tag{1}$$

where $\bar{b}_{n,\mathrm{ref}}$ is the glacier's specific balance in a reference climate and $\bar{b}_n$ is the specific balance in a perturbed climate. This may be expressed in terms of monthly mean precipitation P_k and temperature T_k as:

$$\Delta\bar{b}_n = \sum_{k=1}^{12} \left\{ S_{T,k}(T'_k - \theta) + S_{P,k}(P'_k - \zeta) \right\}, \tag{2}$$

where the $S_{T,k}$ and $S_{P,k}$ are the SSCs for temperature and precipitation respectively, T'_k (P'_k) is the temperature (precipitation) perturbation from the control climate for month k, and θ and ζ are real constants. The temperature SSC is defined as:

$$S_{T,k} = \frac{\partial \bar{b}_n}{\partial T'_k}, \tag{3}$$

and similarly the SSC of precipitation as:

$$S_{P,k} = \frac{\partial \bar{b}_n}{\partial P'_k}, \tag{4}$$

where the precipitation perturbation P'_k from the control climate, at a given month k is:

$$P'_k = \frac{P_k - P_{k,\mathrm{ref}}}{P_{k,\mathrm{ref}}}. \tag{5}$$

The terms θ and ζ are introduced to account for the imbalance between climate and glacier state. It is difficult to quantify these terms in the light of existing information about both the current state of the mass balance of Svalbard's glaciers and climatic conditions in the region. Hence we follow Oerlemans et al. (2005) in setting these to zero. In Sect. 4.2 the $\Delta\bar{b}_n$ under each climate forcing is calculated using $S_{T,k}$ and $S_{P,k}$ from Oerlemans et al. (2005), with T' and P' from the RCM anomalies. This method assumes that changes in SMB are linear with changes in temperature and precipitation, which is reasonable for small perturbations. Here however this not the case, but we use SSCs to provide a first order indication of changes in $\bar{b}_n$ rather than an absolute value or trend.

2.2 Experiment setup and model description

HadRM3 is a limited area model and in this study is "1-way" nested inside HadAM3. Both models employ the same grid scale and sub-grid scale dynamics (Jones et al., 1995; Pope et al., 2000). To account for the differences in horizontal grid resolution, HadAM3 and HadRM3 have dynamical time steps of different lengths. HadAM3 has a time-step of 30 min, with the 0.44° and 0.22° HadRM3 versions having a 5 min and 2.5 min time-step, respectively. The ratio between the resolution of lateral boundary forcing used to force an RCM and the RCM's resolution, is usually between two and five with Denis et al. (2002) suggesting that this ratio should be no larger than ten. When this ratio is too large, multiple nesting is sometimes used, this is where the global model is used to force an intermediate resolution RCM, which is in turn used to force the high resolution RCM (e.g. Christensen et al., 1998). Such a multiple nesting was used in this study since the ratio between the resolution of HadAM3 ($2.5° \times 3.75°$) and HadRM3 (0.22°) is greater than 10. For this purpose a 0.44° HadRM3 simulation was used to force the 0.22° domain.

Lateral boundary forcing of both nested RCM domains are provided by the driving simulation every six hours. These boundary conditions are temporally interpolated by the RCM and updated at each timestep. The SST and sea ice boundary conditions for the RCM and AGCM are interpolated in time from the monthly input data and updated by the model every five days. The SST and sea ice surface forcing for each model was bilinearly interpolated from the HadGEM1 grid onto each model grid.

In both HadRM3 and HadAM3 surface moisture and energy fluxes over land are calculated by the Met Office Surface Exchange Scheme (MOSES). MOSES is a surface hydrology model which calculates moisture and energy fluxes between the atmosphere and its four subsurface/surface levels. Wherever snow or ice is present it is assumed to lie uniformly over the grid cell, changing the thermal conductivity of the surface and reducing surface roughness. Albedo varies between the snow free value (as prescribed from the Wilson and Henderson-Sellers (1985), data set) and the maximum snow covered value, which is 0.8 for temperatures below −2 °C. A complete description of this model component may be found in Cox et al. (1999).

2.3 Validation: methods and data

To identify limitations of the methodology, it is important to validate model performance against observations for the present day. Validation of the RCM temperature and precipitation fields is presented in Sect. 3, where the model was validated against a number of observational data sets. Weather station temperature data are available for four sites in Svalbard, all located in west Spitsbergen. At these locations the seasonal cycle and seasonal mean values were used to validate the model. However, it should be noted that the spatial coverage of such data is sparse and many of the existing records are of short duration. For comparison with observations, the RCM was forced with a climatology of monthly mean SST and sea ice for the period 1961–1990. These were averaged from the MOHC HadISST climatology (Rayner et al., 2003). Forcing the model with this observational data minimises errors in the surface boundary conditions as a source of bias, but not those in the lateral boundary conditions.

There are two permanent meteorological stations in Svalbard: Ny-Ålesund and Longyearbyen, both in west Spitsbergen. A homogenised meteorological record for Longyearbyen is available from 1911-present, and is one of only a few long term temperature records in the Arctic (Nordli and Kohler, 2004). The temperature record from the research base in Ny-Ålesund, which is a coastal site, covers the period 1974–present. In addition, two glaciers with AWS station data are Midtre Lovénbreen and Kongsvegen, both near Ny-Ålesund, west Spitsbergen (see Fig. 1). The Midtre Lovénbreen record lasts from 1997–2002 (Hodson et al., 2005) and Kongsvegen from 2000–2007. Both Midtre

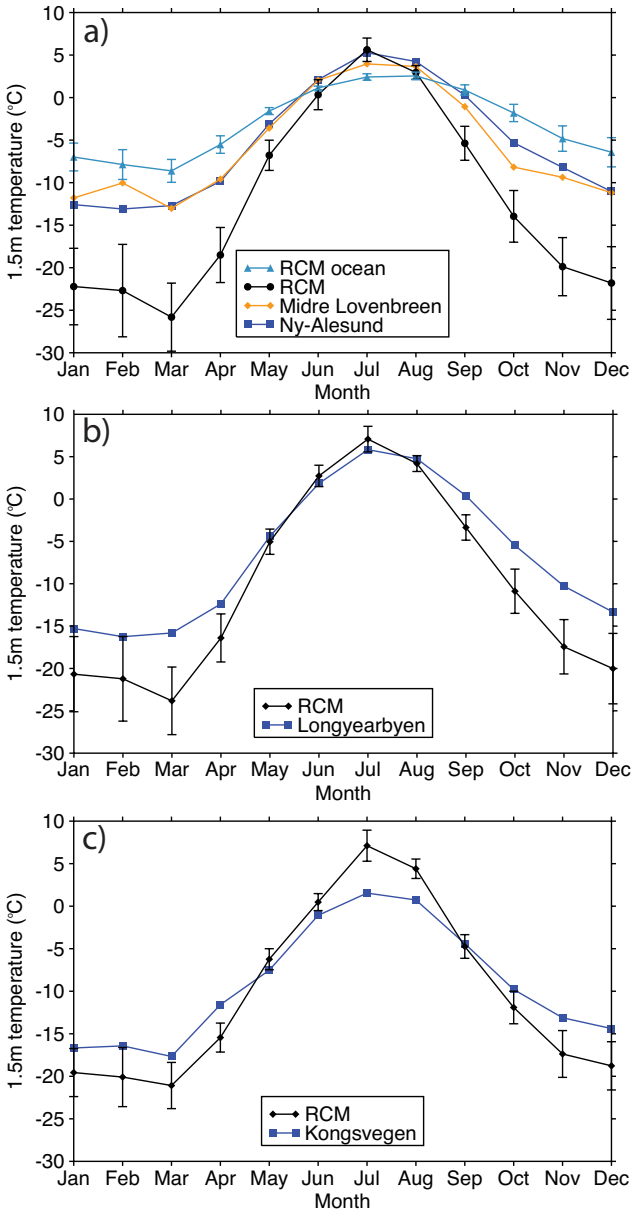

Fig. 3. Modelled and observed mean monthly surface air temperature for, the grid cell containing **(a)** Ny-Ålesund and Midtre Lovénbreen, **(b)** Longyearbyen and **(c)** Kongsvegen. In addition, temperature from the grid cell from the nearest ocean grid cell to Ny-Ålesund is plotted in **(a)** for comparison with the land cell. Each of the RCM mean monthly values have whiskers representing $\pm\sigma$.

Lovénbreen and Ny-Ålesund are contained within a single grid cell.

For comparison with the RCM, a mean monthly temperature climatology was calculated from the available daily observational data at each site. In the case of Longyearbyen, where the record spans the reference period (1961–1990), only data from these years was used. For the other locations, where records are shorter, the whole period of available observations was used. The model data were not lapse rate corrected and each observation was compared with the value of the model grid cell containing it. In addition to these in-situ data, we utilised a five year climatology of melt days for Svalbard for the period 2000–2004, derived from Quick Scatterometer (QSCAT) backscatter data by Sharp and Wang (2009). We used this to validate model temperature spatially. To do this we assume an equivalence of observed melt days and model days where near surface air temperature exceeds 0 °C. This assumed equivalence is justified in that, to a first approximation, when the surface air temperature is positive the surface will be melting, and when the surface air temperature is negative it will not. However, in practice observations of melt are dependent on both satellite overpass time and detection threshold. Also, the 1961–1990 observed mean SSTs and sea ice used to force the RCM are not equivalent to 2000–2004 SSTs and sea ice. Nevertheless, the lack of reliable gridded temperature observations requires us to use proxy data such as these.

Direct observations of precipitation are problematic in cold regions, with rime ice and undercatch seriously impacting the accuracy of measurements (Førland and Hanssen-Bauer, 2003). However, ice cores contain a record of specific net SMB. Pinglot et al. (1999) derived mean, minimum and maximum specific net SMB, b_n for a number of glaciers in Svalbard using the nuclear testing (1963) and Chernobyl (1986) layers as temporal markers.The annual accumulation from these cores forms a lower bound to total precipitation. In Sect. 3.3 we describe the use of these ice core derived accumulation estimates to validate the modelled total precipitation at seven locations.

3 Comparison of model output with observations

As mentioned earlier, there are relatively few long-term meteorological station records in Svalbard and only short records in glaciated areas. Accordingly we also use some proxy data for validation purposes. In this section the 25 km RCM simulation forced with a HadISST derived SSTs and sea ice climatology is validated against these observational data.

3.1 Comparison with meteorological station temperature

Summer temperature is well represented by the RCM at Midtre Lovénbreen and Ny-Ålesund, with residuals of less than 2 °C in all summer months at both locations. In winter however, there is a mean bias of −10 °C at Ny-Ålesund and −11 °C at Midtre Lovénbreen (see Fig. 3a). The RCM performs better at Longyearbyen, where the winter bias is about −7 °C and summer residuals are less than 1.1 °C

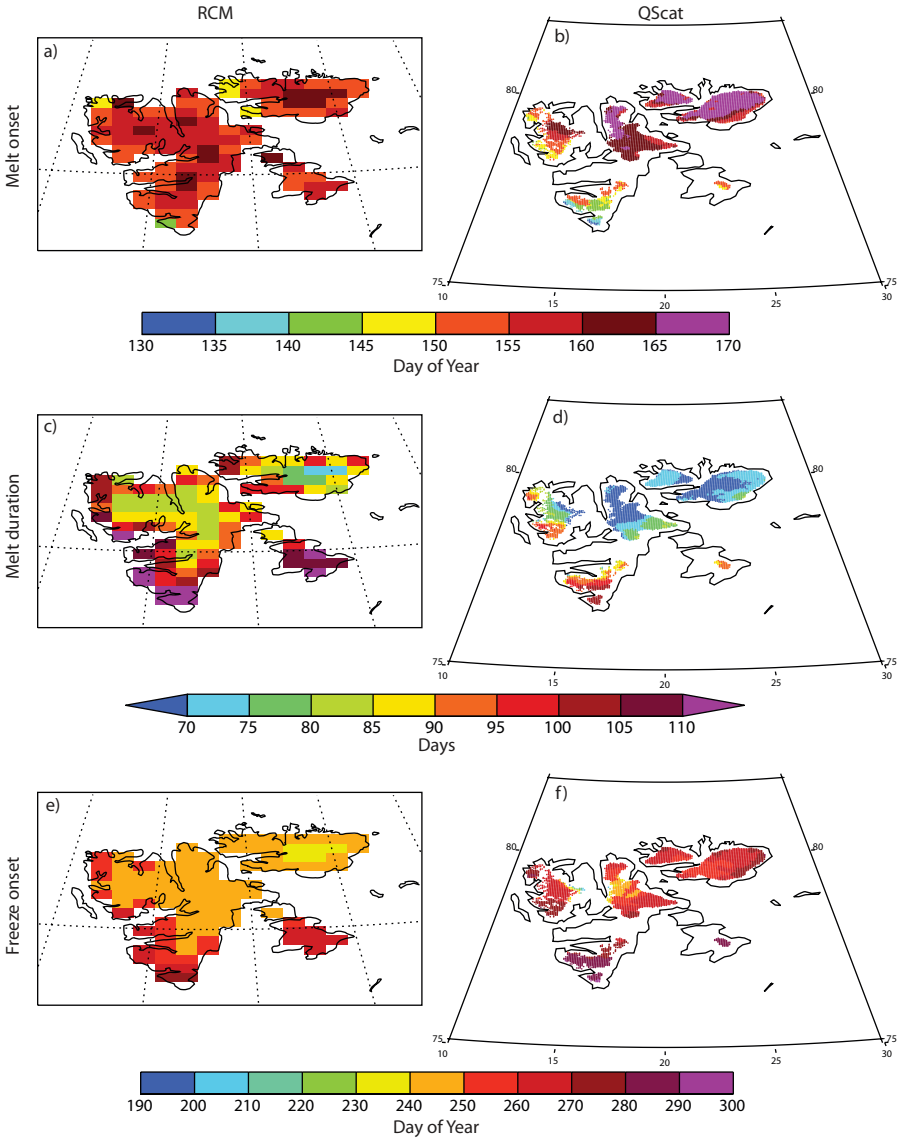

Fig. 4. Modelled and observed climatology of melt onset **(a** and **b)**, melt season duration **(c** and **d)** and freeze onset **(e** and **f)**. The model values are calculated from model days with positive temperatures.

(Fig. 3b). Comparing the mean temperatures in the observational record at Longyearbyen for the period 1961–1990 and 1997–2002, reveals a temperature increase of 3.4 °C in winter and 1.1 °C in summer which accounts for the difference in model bias between this location and Midtre Lovénbreen. This also suggests that the bias at Longyearbyen is more representative.

Annual mean temperature is simulated well by the model at Kongsvegen but the amplitude of the seasonal cycle is small, with a winter cold bias of 3.6 °C and a summer warm bias of 3.5 °C (see Fig. 3c). This apparent winter bias is probably due to an increase in winter temperature of 4.6 °C in west Spitsbergen between the model reference period (1961–1990) and the observational period (2000–2007). Summer temperature also increases between these periods by 1.7 °C, indicating that the summer warm bias is probably larger than this direct comparison suggests. This large seasonality over ice in HadRM3 was discussed by Murphy et al. (2002) when validating model performance over the Greenland ice sheet. Their results suggest that this amplified seasonality is due to the oversimplification of the MOSES albedo scheme over ice.

The prevailing wind direction in Spitsbergen (Ny-Ålesund) is East-South-East, hence the climate on Spitsbergen is dominated by westerly weather systems (Beine et al., 2001). The winter 850 hPa prevailing winds indicate a

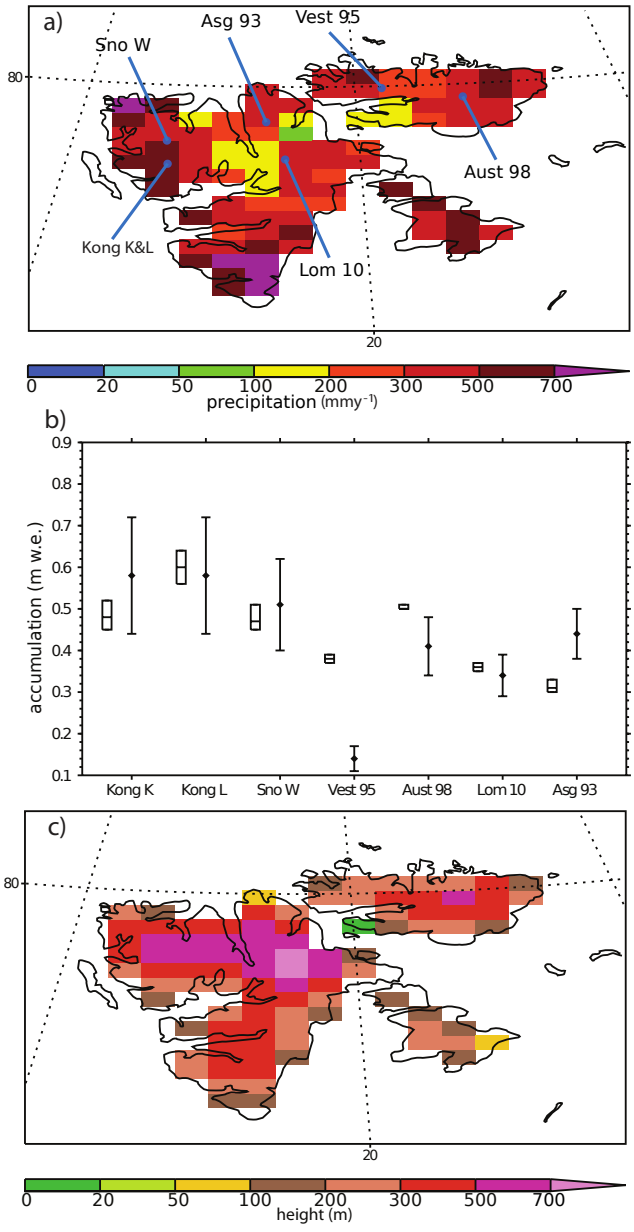

Fig. 5. RCM annual total precipitation and ice core locations (blue), **(a)**, Ice core net accumulation minimum, mean, maximum (box) and RCM total precipitation ($\pm\sigma$, whiskers), **(b)**, and RCM orographic height, **(c)** .

$\sim$1 m s^{-1} south-westerly bias when compared with ERA-40, which cannot explain the winter cold bias. The seasonal cycle of temperature at Midtre Lovénbreen and Ny-Ålesund follows the nearest ocean cell in the RCM better than the containing land cell (Fig. 3a). This indicates that the model is not capturing the marine climate at these locations. A similar winter bias in Longyearbyen and Ny-Ålesund is present in the REMO$_{iso}$ RCM and is thought to be caused by an overestimation of boundary layer inversion strength (Divine et al., 2011b). This is thought to be caused by the low resolution of the model, which does not sufficiently represent the coastal location of these meteorological stations and their proximity to open water. Similar deficiencies in boundary layer processes may also explain the winter cold bias in HadRM3.

3.2 Melt climatology

In the following section, RCM positive temperature days are compared with the surface melt climatology from QSCAT (Sharp and Wang, 2009). For each RCM grid cell, the period between the first and last days of the year with positive daily mean near surface temperature are referred to as the melt season. The RCM models the onset of melt, melt duration and freeze onset well across most of south and west Spitsbergen (Fig. 4). Melt data are not available near Longyearbyen or Ny-Ålesund, but the observed melt season duration near Kongsvegen is shorter than is simulated by the model. This is consistent with in-situ observed temperatures at this location, discussed in Sect. 3.1, which also show that temperatures are above zero for a shorter period of time than simulated by the model. In east Spitsbergen melt starts too early by 5–20 days and freeze onset is 0–10 days too early depending on the location. This results in a melt season which is 0–20 days too long and indicates that the model's cold bias in Longyearbyen and Ny-Ålesund may be very localised. Melt in Nordaustlandet starts 10–30 days early and freeze onset is 10–20 days too early, leading to a melt season which is 5–25 days too long depending on the location. This indicates that this area experiences a warm bias near the beginning and end of the melt season. Between the 1961–1990 period used to force the RCM and the 2000–2004 period used to produce the climatology of Sharp and Wang (2009) there has been a general retreat in sea ice and increase in SST. This likely explains at least part of the difference between these melt climatologies in Nordaustlandet.

3.3 Accumulation validation

Ice core derived specific net SMB for the periods listed in Table 1 were used to validate modelled total precipitation (Pinglot et al., 1999). These values are compared to modelled annual mean precipitation in the grid cells containing each of the seven core sites (see Tables 1, 2 and Fig. 5a). The results indicate that the RCM has ample precipitation at all five locations on Spitsbergen but underestimates precipitation at both sites on Nordaustlandet (Fig. 5b); at the Aust 98 and Vest 95 sites the model simulates 82 % and 37 % of that observed respectively (see Table 2). Observations on the Vestfonna ice cap indicate that accumulation is almost exclusively controlled by altitude (Möller et al., 2011a,b). Thus, the insufficient level of model precipitation could be due to the low model orography on Nordaustlandet, which is over 300 m below the actual height of the Vest 95 ice core site (see Table 2 and Fig. 5c). Vestfonna lies on the leeward side

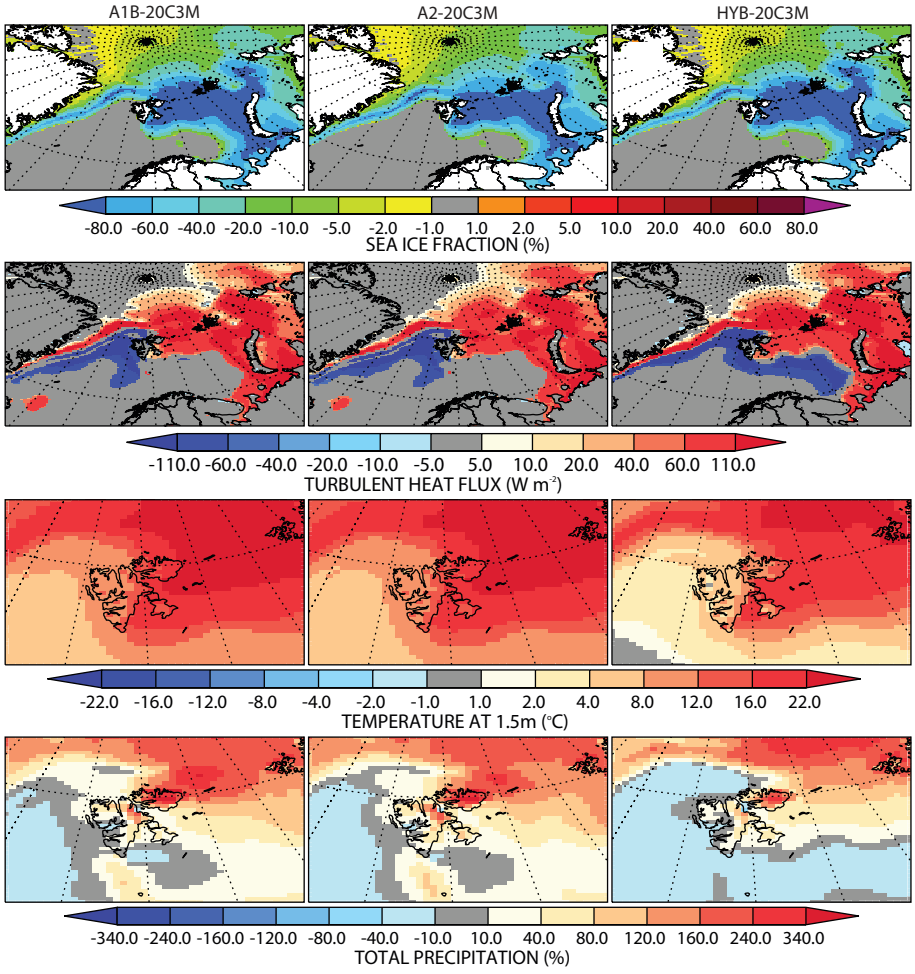

Fig. 6. Winter anomalies of sea ice concentration (%), turbulent heat flux (W m^{-2}), surface air temperature (°C) and total precipitation (%) of the A1B, A2 and HYB from the 20C3M simulation. Apart from sea ice, anomalies are significant at the 95 % level using a student's *t*-test.

Table 1. Ice core name, location, altitude, equilibrium line altitude and the period the ice core covers for the ice core sites used in this study (from Pinglot et al., 1999).

Glacier	Ice core	long	lat	Alt. (m)	ELA (m)	Period
Kongsvegen	Kong K	13.28	78.78	639	520	1963–1988
	Kong L	13.45	78.77	726	520	1965–1991
Snøfjella	Sno W	13.28	79.13	1190	650	1963–1991
Vestfonna	Vest 95	21.02	79.97	600	505	1963–1994
Austfonna	Aust 98	24.00	79.80	740	505	1963–1997
Lomonosovfonna	Lom 10	17.42	78.87	1230	660	1963–1996
Åsgårdfonna	Asg 93	16.72	79.45	1140	800	1963–1992

of Austfonna but in the model these features are not topographically distinct. This will also cause inaccuracies in the representation of precipitation patterns at this resolution.

Accumulation rates on Svalbard are extremely variable both spatially and temporally, with accumulation experiencing large inter-annual variation (Sand et al., 2003). Because of this, only limited information can be derived from

Table 2. Specific net SMB average, minimum and maximum estimates from ice cores and RCM annual total precipitation and standard deviation. The altitude of the ice core location, the RCM grid cell orographic height and the difference between RCM precipitation and ice core accumulation are included.

	Ice core				RCM			
		SMB (m w.e.)				Precipitation (m)		
Ice core	Alt.(m)	Ave.	Min.	Max.	Alt.(m)	Ave.	σ	diff. Ave.
Kong K	639	0.48	0.45	0.52	474	0.58	0.14	0.10
Kong L	726	0.60	0.56	0.64	474	0.58	0.14	−0.02
Sno W	1190	0.47	0.45	0.51	604	0.51	0.11	0.04
Vest 95	600	0.38	0.37	0.39	271	0.14	0.03	−0.24
Aust 98	740	0.50	0.50	0.51	502	0.41	0.07	−0.09
Lom 10	1230	0.36	0.35	0.37	725	0.34	0.05	−0.02
Asg 93	1140	0.31	0.30	0.33	538	0.44	0.06	0.13

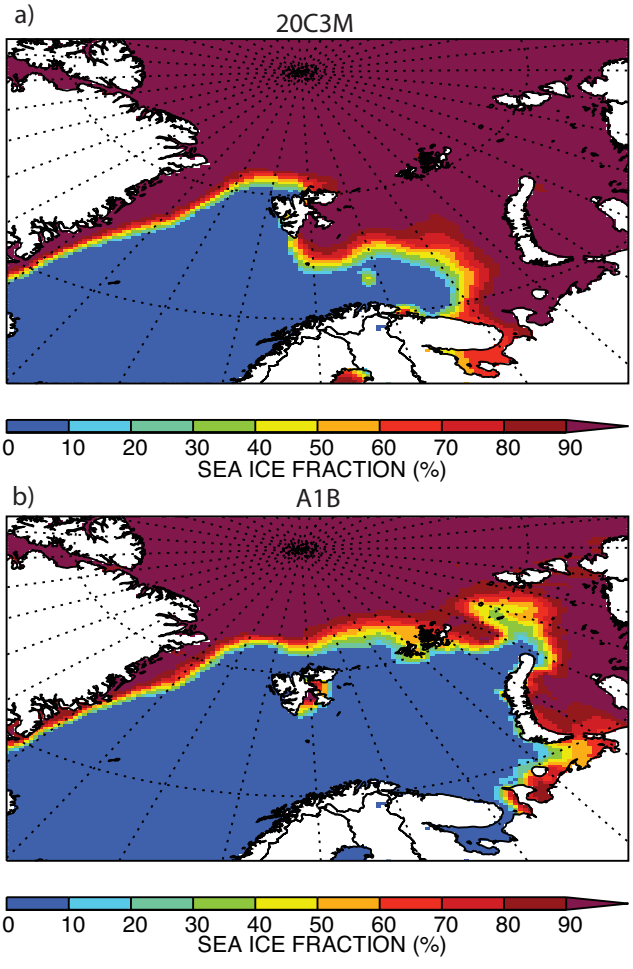

Fig. 7. March (maximum) mean sea ice concentration for **(a)**, 20C3M experiment and **(b)** A1B experiment. Interpolated onto the 0.22° RCM grid from the HadGEM1 CMIP3 experiments.

the comparison of these point accumulation values with the RCM's 25 km grid values. This highlights the issues surrounding the comparison of point data with grid cell model data (e.g. Skelly and Henderson-Sellers, 1996) when the level of real surface inhomogeneity is large, as it is in Svalbard. Nonetheless, this comparison does provide some confidence that the large scale features of precipitation across Svalbard are captured by the model.

4 The impact of changes in sea ice to the climate of Svalbard

The previous section showed that although the model has limitations, it does successfully represent aspects of Svalbard's climate which are relevant to SMB. In this section we will first present the impacts of 21st Century sea ice changes on the surface energy balance of the ocean surrounding Svalbard and Svalbard's temperature and total precipitation. Secondly, we describe the impact of these changes on the SMB of Svalbard's glaciers and ice caps using the SSC method described in Sect. 2.1.

4.1 Energy balance, hydrological cycle and temperature

One of the areas predicted to experience a rapid sea ice retreat is around Svalbard (Fig. 6). The archipelago is intersected by the March sea ice edge in the 20C3M present day experiment and sea ice covers most of the Barents sea. In all future scenarios the March sea ice edge has migrated north past the 80° latitude band, leaving open water to Svalbard's north and eastern shores (Fig. 7). During the sea ice minimum extent in September of the 20C3M climatology, the sea ice edge reaches the northeastern coast of the Svalbard archipelago. In the future scenarios the Arctic Ocean is almost completely ice-free, other than some small protected areas around the north coast of Greenland and the Canadian archipelago.

Turbulent heat flux (THF) is used here to refer to the sum of positive upward latent and sensible heat fluxes from the surface. In all three future simulations, there are large increases in THF over areas experiencing a reduction in sea ice concentration. This is most pronounced in winter, since the atmosphere is coldest relative to the ocean in this season. There is a dipole pattern in the winter THF anomaly, with positive anomalies between the 20C3M and future sea ice edge and negative anomalies south of the 20C3M sea ice edge. The area south of the sea ice edge is a local maximum of THF field, since the open ocean is in contact with extremely cold polar air (Fig. 6). In the reduced sea ice scenarios, this local maximum occurs on the seaward side of the future sea ice edge, this effect was also observed in the study of Deser et al. (2010). The sea ice edge in the 20C3M winter climatology lies close to Svalbard, such that in reduced sea ice scenarios the ocean to the south west experiences less THF, while the water around the northeastern coast experiences a larger THF. The areas of largest increase are in the Barents and Kara Seas, where winter anomalies are over $110\,\mathrm{Wm}^{-2}$ in places (Fig. 6).

Both A1B and A2 simulations show large winter temperature increases across Svalbard compared to 20C3M, with temperatures increasing by as much as 21 °C in north east Nordaustlandet. This compares to a global temperature change of 2.8 °C and 3.0 °C for these scenarios, respectively. There is a large gradient of change between the west coast of Spitsbergen and Nordaustlandet, with the west coast experiencing more moderate changes of 8 °C. The decline of sea ice around the eastern side of the archipelago amplifies warming in this region. Changes are more moderate in HYB as one might expect, with changes of 0–15 °C between the west and east coast (see Table 3 and Fig. 6). This is the portion of the change which is due to the impact of sea ice declining in this region. This indicates that sea ice decline alone is responsible for at least ∼66 % of the winter warming in the A1B scenario.

The resulting changes to winter precipitation are also dramatic, with A1B and A2 showing precipitation anomalies of more than 400 % over Nordaustlandet compared to 20C3M (Fig. 6 and Table 3). These changes are the result of an altered hydrological cycle in the region, due to the previously described changes in THF, as well as changes in circulation, with the winter prevailing wind direction changing from predominantly north west to south west (not shown). This southerly shift in wind direction over Svalbard is caused by the change in thermal gradient over the Barents and Kara Seas. Similarly to temperature, changes in precipitation under the A1B and A2 scenarios have a large north east to south west gradient. Nordaustlandet and east Spitsbergen experience large increases in precipitation, whereas western Spitsbergen experiences less change. Some coastal locations near Isfjorden even experience a small reduction in precipitation. Whilst warmer temperatures in the region mean that there is more moisture transport and precipitation over the archipelago, the reduced THF in the Greenland sea to the west coast of Spitsbergen causes this decrease in precipitation along parts of the east coast. The relatively low prevailing wind speeds in the Arctic mean that the anomalies of precipitation for both winter and summer closely follow the anomalies of THF, especially in the HYB experiment. The precipitation anomaly caused by sea ice decline in HYB has a clear dipole pattern, with areas of increased THF having increased precipitation and negative THF areas, reduced precipitation (Fig. 6).

Svalbard experiences a more moderate increase in winter precipitation of ∼54 % in HYB but the anomalies have similar spatial pattern to the A1B and A2 experiments. There are small negative changes around west Spitsbergen and large changes (∼270 %) over Nordaustlandet (Fig. 6). The changes in precipitation in HYB are the result of changes in THF caused by sea ice decline. These are more localised to the areas of ice decline than the A1B anomaly, which includes the impact of both global and Arctic increases in SST. Changes in precipitation due to large scale changes in global atmospheric moisture content and transport associated with global warming are excluded from the HYB simulation by design.

The areas north of Svalbard and Franz Joseph Land experience the largest reduction in sea ice between the 20C3M and future climates (Fig. 8). The reduction in sea ice concentration over the Barents Sea in summer is less than in winter, this is because in 20C3M the Barents Sea has lower concentrations than in the winter, when more grid cells are 100 % ice covered. Because of this, the HYB experiment's summer THF response due to sea ice reduction alone is small and negative over some areas where ice is removed. This is because the SST in these grid cells was set to −1.8 °C, which is colder than the near surface air temperature above sea ice in the 20C3M simulation (see HYB in Fig. 8). However the response to sea ice decline and SST increase in the A1B and A2 experiments is more noticeable with increased THF where sea ice has retreated. The area with the largest increase is north of Svalbard on the seaward side of the future sea ice edge.

The summer temperature response in the HYB experiment is small with some isolated decreases in temperature. The A1B and A2 temperature responses are more significant, with positive anomalies of 0–5 °C, with changes located mainly in southern Spitsbergen and Edgeøya. This compares to global temperature changes of 2.3 °C and 2.55 °C for each respective scenario. Similarly, compared to winter the summer changes to precipitation are relatively small in HYB (between −30 % and −40 % in some areas) with positive changes in the north and negative changes in some southern and central areas. When SST changes are included precipitation more than doubles in some areas with the largest changes occurring in northeastern Spitsbergen and Nordaustlandet. More moderate increases occur on the west coast of Spitsbergen. This is driven by both increased THF from the

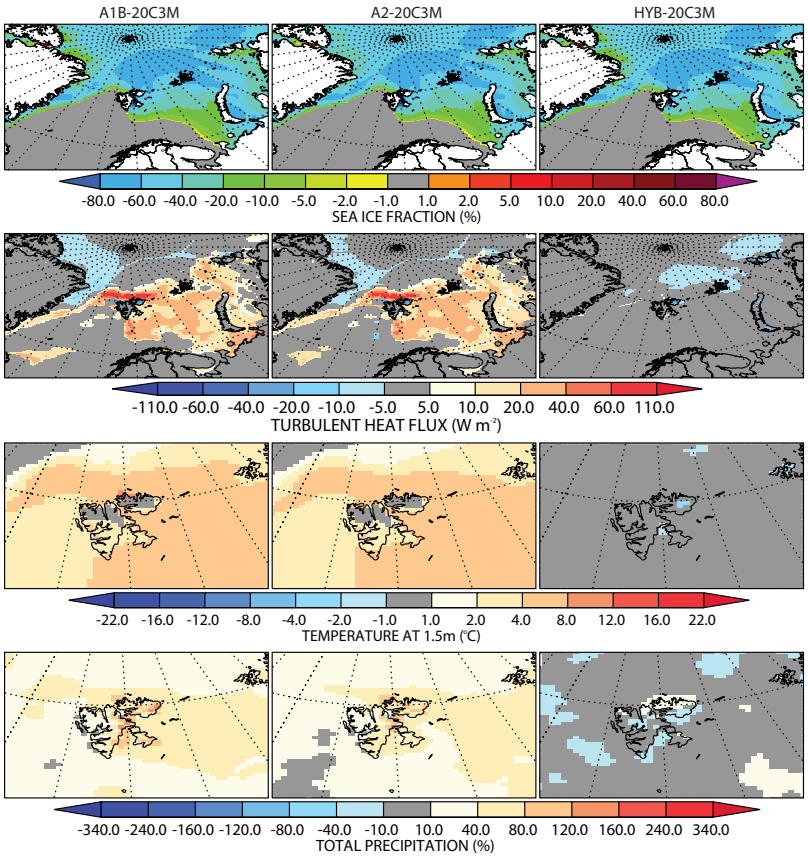

Fig. 8. Summer anomalies of sea ice concentration (%), turbulent heat flux (W m^{-2}), surface air temperature (°C) and total precipitation (%) of the A1B, A2 and HYB from the 20C3M simulation. Apart from sea ice, anomalies are significant at the 95 % level using a student's *t*-test.

Table 3. Annual (ANN), Spring (MAM), Summer (JJA), Autumn (SON) and winter (DJF) estimates of area averaged temperature and total precipitation change on Svalbard for A1B, A2 and HYB simulations, compared to 20C3M control experiment. The intervals expresses the geographical spread of change, not projection uncertainty.

Field	Season	A1B	A2	HYB
Temperature (°C)	ANN	5–12	6–12	0–6
	MAM	5–11	6–12	0–7
	JJA	0–5	0–5	−3–0
	SON	6–13	6–13	0–5
	DJF	8–21	8–21	0–15
Precipitation (%)	ANN	−9–232	−4–213	−14–101
	MAM	−19–264	−7–216	−20–148
	JJA	14–125	10–105	−29–38
	SON	−25–201	−21–233	−32–47
	DJF	−17–445	−10-446	−13–273

Arctic Ocean and poleward moisture transport from lower latitudes. The temperature and precipitation response in the A1B and A2 simulations is similar to Rinke and Dethloff (2008) and the THF response in HYB is similar to Deser et al. (2010). This is encouraging and provides confidence in the robustness of these results.

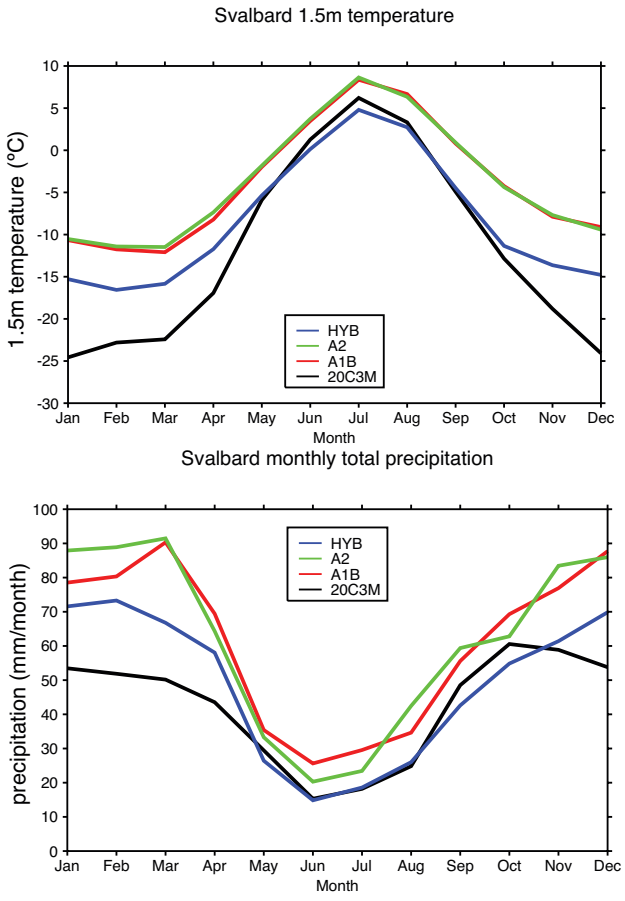

Fig. 9. Svalbard's monthly mean (area averaged) cycle of surface air temperature (°C), **(a)**, and total precipitation (mm/month), **(b)**.

4.2 Surface mass balance

For each experiment, A1B, A2 and HYB, the change in specific balance, $\Delta\bar{b}_n$, of the total land ice across the archipelago was calculated based on the SSCs of Oerlemans et al. (2005) (Fig. 2). They were calculated using Eq. (2), where the changes in precipitation and temperature were area averaged across the whole of Svalbard and the reference climate was the 20C3M experiment. For A1B, A2 and HYB the values of $\Delta\bar{b}_n$ are -0.31 m water equivalent (w.e.), -0.31 m w.e. and 0.35 m w.e. respectively. In the A1B and A2 experiments the $\Delta\bar{b}_n$ is dominated by increased melt, resulting from increases in the melt season temperature (Fig. 9a). Precipitation increases throughout the year, especially in winter months and while this compensates the melt driven mass loss to some extent, the increase is not enough to avoid a negative $\Delta\bar{b}_n$ (Fig. 9b). In reality an increase in summer liquid precipitation would act as a heat gain to the surface and causes melt, an effect that is not accounted for by the SSCs and one that would result in an even more negative change in $\bar{b}_n$, in both A1B and A2 experiments.

The HYB experiment experiences a net increase in $\bar{b}_n$, which is caused by both a decrease in melt season temperature, which causes less melt and an increase in winter precipitation (Fig. 9b). There is a decrease in summer precipitation but the SSC method is not sensitive to changes in accumulation during the melt season and this is more than compensated by increases in accumulation in winter (Fig. 2). Significant increases in temperature occur outside of the present day melt season between September–May; these do not affect the calculated change in $\bar{b}_n$ since the values of $S_{T,k}$ are zero in these months, indicating no change in melt. However, this will not be the case if temperatures rise above the melting point. This suggests that this method will underestimate $\Delta\bar{b}_n$ for large perturbations in temperature, such as those presented here.

5 Conclusions

5.1 Model validation

Most of the GCMs used to model global change in the IPCC AR4 report have insufficient resolution to adequately simulate changes in climate and glacial mass balance in regions of complex topography like Svalbard (e.g. Meehl et al., 2007). This has motivated the use of RCMs to downscale climate projections (Christensen et al., 2007). In this study we demonstrated that the 25 km (0.22°) version of HadRM3 performs well in reproducing some aspects of Svalbard's climate in the present day. The model was validated against in-situ meteorological station data from the Norsk Polarinstitutt research station at Ny-Ålesund and AWS data from the near by glaciers Midtre Lovénbreen and Kongsvegen as well data for Longyearbyen airport, near Isfjorden.

The RCM performed well against observations in summer with residuals from observations less than 2 °C at all stations but Kongsvegen, where residuals were less than 6 °C. However, in winter the climate was dominated a cold bias of ∼7 °C in west Spitsbergen, probably associated with a strong boundary layer inversion in the model. Even at 25 km the model orography was not adequately resolved to represent coastal atmospheric circulation and could partly explain the strength of this inversion.

RCM precipitation was validated against net accumulation derived from ice cores (Pinglot et al., 1999). The model performs well at all five sites on Spitsbergen but precipitation is too low at both sites on Nordaustlandet. Low levels of model precipitation on Nordaustlandet may be associated with the relatively low resolution representation of orography on the (25 km) HadRM3 grid. As such, future climate modelling studies of Svalbard would benefit from the use of higher resolution models.

The use of the melt season climatology of Sharp and Wang (2009) as a means to validate the RCM is unusual, but it provides information about temperature during the melt season in regions which don't have in situ observation. We decided against regridding the data onto the same grid as the RCM or vice versa and performing more robust statistical tests since the two quantities are not strictly equivalent. The differences in climate state between both the modelled period and period of observation also inhibit a fair comparison of these quantities. Nonetheless, in regions of sparse observations, the data provides some qualitative assessment, indicating that temperatures in east Spitsbergen and Nordaustlandet are too warm near the onset and end of the melt season.

5.2 Climate change and mass balance

This study has investigated the impact of 21st Century sea ice decline on the temperature, precipitation and SMB of Svalbard's ice caps and glaciers. A novel experiment was conducted with the RCM to separate the impact of sea ice decline on Svalbard's climate and SMB from the impact of increased global SST. Sea ice decline was shown to have a large effect on ocean surface energy flux, especially in winter where the near surface air temperature is coldest relative to the ocean.

We found that ∼66 % of the winter warming and ∼54 % of the increase in precipitation between the 20C3M (1961–1990) and the A1B (2061–2090) scenario was caused by sea ice decline. In summer, sea ice decline causes relatively little change in both temperature and precipitation over Svalbard compared to winter. When changes in SST are also included, the net effect in the A1B and A2 simulations is a significant increase in both precipitation and temperature in all seasons.

The changes in temperature and precipitation for the Barents Sea region in the A1B and A2 simulations in this study are larger than the estimates of Førland et al. (2009). This is not surprising since they performed their simulations under the more moderate B2 scenario. However, our temperature prediction is similar to Rinke and Dethloff (2008) who also used A1B forcing. This provides some confidence in the magnitude of simulated change. The seasonality of changes in precipitation and temperature are similar to both these studies. However, it should be noted that the periods of analysis are not consistent between these experiments.

When SSTs are fixed to 20C3M values, sea ice decline causes a net increase in the mass balance of Svalbard's glaciers. The HYB experiment shows a decrease in summer temperature and an increase in annual precipitation, leading to a positive net change in specific SMB averaged across the archipelago of 0.35 m w.e. This is in stark contrast to the coupled effect in the A1B simulation which shows a net decrease in SMB −0.31 m w.e. Both these changes are similar in magnitude to the present day mass balance for Svalbard (=−0.36 m a^{-1} w.e., excluding Austfonna and Kvitøya) (Nuth et al., 2010). These results suggest that although Svalbard's glaciers will experience increased accumulation due to both sea ice decline and an increase in poleward moisture transport, this will not balance the enhanced melt due to increased temperature. However in the future this sea ice related increase in accumulation may moderate the impact of increased melting for glaciers both in Svalbard and other areas in the vicinity of declining sea ice.

The magnitude of change in the A1B and A2 scenarios is similar since the emission trajectories lead to similar changes in Arctic SST and sea ice cover over the period used to force the RCM. The largest change in surface temperature between the 20C3M reference climate and these future climates is due to the change in sea ice, which is a feature of both scenarios (Nakicenovic and Swart, 2000). There are some differences in global SST which cause small differences in both the climate and SMB of Svalbard.

Fixing SSTs in the HYB experiment to present day values makes it possible to isolate the impact of sea ice decline on Svalbard's climate and SMB. There is little difference in the atmospheric vertical velocities over the Arctic Ocean between the A1B and HYB experiments (not shown). This indicates that vertical moisture transport from the ocean surface into the lower atmosphere is realistic in HYB. However, using this method we cannot determine if the redistribution of this moisture is realistic. It may not be, since differences between the 20C3M and A1B storm tracks and wind fields will have some effect on this and are not included in the HYB simulation. It is also hard to interpret the HYB temperature field, which is physically inconsistent with the sea ice.

The SSC method was used to assess the change in mass balance due to the impact of climate change (Oerlemans et al., 2005). This assumes that $\bar{b}_n$ changes linearly with temperature and precipitation change and does not take into account nonlinearity in the response of melt to temperature for temperatures close to the melting point. As such, the SSC method likely underestimates the change in melt given the large simulated increase in temperature over Svalbard. Using an energy balance model would be a more robust approach to modelling the impact of climate change on glacier SMB. However, this would require downscaling to higher resolution (1–5 km) in order to capture the characteristic fjord-type topography of outlet glaciers in Svalbard. Nevertheless, the SSC method provides a qualitative indication of the SMB anomaly that would result from sea ice decline.

Acknowledgements. This work was carried out using the computational facilities of the Advanced Computing Research Centre, University of Bristol – http://www.bris.ac.uk/acrc/. Assistance in using HadRM3 was provided by the National Center for Atmospheric Science (NCAS). We acknowledge the modelling groups, the Program for Climate Model Diagnosis and Intercomparison (PCMDI) and the WCRP's Working Group on Coupled Modelling (WGCM) for their roles in making available the WCRP CMIP3 multi-model dataset. Support of this dataset is provided by the Office of Science, US Department of Energy. We thank Martin Sharp, University of Alberta, Andy Hodson, University of Sheffield and Hans Oerlemans, Institute for Marine and Atmospheric

research, Utrecht, for providing data for this study. We also thank the Jeff Ridley, Xavier Fettweis and one anonymous reviewer for their comments and insight, which has significantly improved the final manuscript.

Edited by: E. Hanna

References

Arendt, A. A., Echelmeyer, K. A., Harrison, W. D., Lingle, C. S., and Valentine, V. B.: Rapid Wastage of Alaskan Glaciers and their Contribution to Rising Sea Level, Science, 297, 382–386, 2002.

Bamber, J., Krabill, W., Raper, V., and Dowdeswell, J.: Anomalous recent growth of part of a large Arctic ice cap: Austfonna, Svalbard, Geophys. Res. Lett., 31, L12402, doi:10.1029/2004GL019667, 2004.

Banta, J. R. and McConnell, J. R.: Annual accumulation over recent centuries at four sites in central Greenland, J. Geophys. Res.-Atmos., 112, D10114, doi:10.1029/2006JD007887, 2007.

Benestad, R. E., Førland, E. J., and Hanssen-Bauer, I.: Empirically downscaled temperature scenarios for Svalbard, Atmos. Sci. Lett., 3, doi:10.1006/asle.2002.0050, 2002.

Benestad, R. E., Hanssen-Bauer, I., Torill, E. S., and Førland, E. J.: Associations between the sea-ice and the local climate on Svalbard, 7 klima, met.no, 2002.

Beine, H. J, Argentini, S., Maurizi, A., Mastrantonio, G., and Viola, A.: The local wind field at Ny-Alesund and the Zeppelin mountain at Svalbard, Meteorol. Atmos. Phys., 78, 107–113, 1–2, 2001.

Boé, J. L., Hall, A., and Qu, X.: September sea-ice cover in the Arctic Ocean projected to vanish by 2100, Nat. Geosci., 2, 341–343, 2009.

Christensen, O. B., Christensen, J. H., Machenhauer, B., and Botzet, M.: Very high-resolution regional climate simulations over Scandinavia – Present climate, J. Climate, 11, 3204–3229, 1998.

Christensen, J. H., Hewitson, B., Busuioc, A., Chen, A., Gao, X., Held, I., Jones, R., Kolli, R. K., Kwon, W.-T., Laprise, R., Magaa, V. Rueda, Mearns, L.,Menndez, C. G., Risnen, J., Rinke, A., Sarr, A., and Whetton, P.: Regional Climate Projections, in: Climate Change 2007: The Physical Science Basis. Contribution of Working Group I to the Fourth Assessment Report of the Intergovernmental Panel on Climate Change, edited by: Solomon, S., Qin, D., Manning, M., Chen, Z., Marquis, M., Averyt, K. B., Tignor, M., and Miller, H. L., Cambridge University Press, Cambridge, United Kingdom and New York, NY, USA, 2007.

Cox, P. M., Betts, R. A., Bunton, C. B., Essery, R. L. H., Rowntree, P. R., and Smith, J.: The impact of new land surface physics on the GCM simulation of climate and climate sensitivity, Clim. Dynam., 15, 183–203, 1999.

Denis, B., Laprise, R., Caya, D., and Cote, J.: Downscaling ability of one-way nested regional climate models: the Big-Brother Experiment, Clim. Dynam., 18, 627–646, 2002.

Deser, C., Tomas, R., Alexander, M., and Lawrence, D.: The Seasonal Atmospheric Response to Projected Arctic Sea Ice Loss in the Late Twenty-First Century, J. Climate, 23, 333–351, 2010.

Divine, D. V. and Dick, C.: Historical variability of sea ice edge position in the Nordic Seas, J. Geophys. Res.-Ocean, 111, C01001, 14 pp., doi:10.1029/2004JC002851, 2006.

Divine, D., Isaksson, E., Martma, T., Meijer, H. A. J., Moore, J., Pohjola, V., van de Wal, R. S. W., and Godtliebsen, F.: Thousand years of winter surface air temperature variations in Svalbard and northern Norway reconstructed from ice-core data, Polar Res., 30, 7379, doi:10.3402/polar.v30i0.7379, 2011.

Divine, D. V., Sjolte, J., Isaksson, E., Meijer, H. A. J., van de Wal, R. S. W., Martma, T., Pohjola, V., Sturm, C., and Godtliebsen, F.: Modelling the regional climate and isotopic composition of Svalbard precipitation using REMOiso: a comparison with available GNIP and ice core data, Hydrol. Process., 25, 3748-3759, doi:10.1002/hyp.8100, 2011.

Dyurgerov, M., Bring, A., and Destouni, G.: Integrated assessment of changes in freshwater inflow to the Arctic Ocean, J. Geophys. Res.-Atmos., 115, D12116, 9 pp., doi:10.1029/2009JD013060, 2010.

Feser, F.: Enhanced Detectability of Added Value in Limited-Area Model Results Separated into Different Spatial Scales, Mon. Weather Rev., 134, 2180–2190, doi:http://dx.doi.org/10.1175/MWR3183.1, 2006.

Førland, E. J. and Hanssen-Bauer, I.: Climate variations and implications for precipitation types in the Norwegian Arctic, 24/02 klima, met.no, 2003.

Førland, E. J., Hanssen-Bauer, I. and Nordli, P. Ø.: Climate statistics and longterm series of temperatures and precipitation at Svalbard and Jan Mayen, DNMI 21/97 klima, met.no, 1997.

Førland, E. J., Benestad, R. E., Flatøy, F., Hanssen-Bauer, I., Haugen, J. E., Isaksen, K., Sorteberg, A., and Ådlaandsvic, B.: Climate development in North Norway and the Svalbard region during 1900–2100, Norwegian Polar Institute, Report series no. 128, 44 pp., 2009.

Hagen, J. O., Liestøl, O., Roland, E., and Jorgensen, T.: Glacier Atlas of Svalbard an Jan Mayan, Norsk Polarinstitutt Meddelelser, 129, 141 pp., 1993.

Hagen, J. O., Melvold, K., Pinglot, F., and Dowdeswell, J. A.: On the Net Mass Balance of the Glaciers and Ice Caps in Svalbard, Arct. Antarct. Alp. Res., 35, 2, 264–270, 2003.

Hanssen-Bauer, I. and Førland, E.: Verification and analysis of a climate simulation of temperature and pressure fields over Norway and Svalbard, Clim. Res., 16, 225–235, 2001.

Hodson, A. J., Kohler, J., Brinkhaus, M., and Wynn, P.: Multi-year water and surface energy budget of a high-latitude polythermal glacier: evidence for overwinter water storage in a dynamic subglacial reservoir, Ann. Glaciol., 42, 42–46, 2005.

Isaksson, E., Divine, D., Kohler, J., Martma, T., Pohjola, V., Motoyama, H., and Watanabe, O.: Climate oscillations as recorded in Svalbard ice core delta O-18 records between AD 1200 and 1997, Geogr. Ann. A., 87A, 203–214, 2005a.

Isaksson, E., Kohler, J., Pohjola, V., Moore, J., Igarashi, M., Karlf, L., Martma, T., Meijer, H., Motoyama, H., Vaikme, R., and van de Wal, R. S. W.: Two ice-core 18O records from Svalbard illustrating climate and sea-ice variability over the last 400 years, The Holocene, 15, 501–509, 2005b.

Jones, R. G., Murphy, J. M., and Noguer, M.: Simulation of Climate-Change over Europe Using a Nested Regional-Climate Model .1. Assessment of Control Climate, Including Sensitivity to Location of Lateral Boundaries, Q. J. Roy. Meteor. Soc., 121, 1413–1449, 1995.

Kaser, G., Cogley, J. G., Dyurgerov, M. B., Meier, M. F., and

Ohmura, A.: Mass Balance of Glaciers and Ice Caps: Consensus Estimates for 1961–2004, Geophys. Res. Lett., 33, L19501, 5 pp., doi:10.1029/2006GL027511, 2006.

Liestøl, O.: Glaciers of Svalbard, Norway, Satellite Image Atlas of Glaciers of the World, USGS Professional Paper 1386-E-5, 1993.

Meehl, G. A., Stocker, T. F., Collins, W. D., Friedlingstein, P., Gaye, A. T., Gregory, J. M., Kitoh, A., Knutti, R., Murphy, J. M., Noda, A., Raper, S. C. B., Watterson, I. G., Weaver, A. J., and Zhao, Z.-C.: Global Climate Projections, in: Climate Change 2007: The Physical Science Basis. Contribution of Working Group I to the Fourth Assessment Report of the Intergovernmental Panel on Climate Change, edited by: Solomon, S., Qin, D., Manning, M., Chen, Z., Marquis, M., Averyt, K. B., Tignor, M., and Miller, H. L., Cambridge University Press, Cambridge, UK, NY, USA, 2007

Meier, M. F., Dyurgerov, M. B., Rick, U. K., O'Neel, S., Pfeffer, W. T., Anderson, R. S., Anderson, S. P., and Glazovsky, A. F.: Glaciers dominate Eustatic sea-level rise in the 21st century, Science, 317, 1064–1067, 2007.

Moholdt, G., Nuth, C., Hagen, J. O., and Kohler, J.: Recent elevation changes of Svalbard glaciers derived from ICESat laser altimetry, Remote Sens. Environ., 114, 11, 2756–2767, doi:10.1016/j.rse.2010.06.008, 2010.

Möller, M., Finkelnburg, R., Braun, M., Hock, R. and Jonsell, U., Pohjola, V. A., Scherer, D., and Schneider, C.: Climatic mass balance of the ice cap Vestfonna, Svalbard: A spatially distributed assessment using ERA-Interim and MODIS data, J. Geophys. Res., 116, F03009, doi:10.1029/2010JF001905, 2011.

Möller, M., Möller, R., Beaudon, R., Mattila, É., Finkelnburg, O. P., Braun, R., Grabiec, M., Jonsell, M., Luks, U., Puczko, B., Scherer, D., and Schneider, C.: Snowpack characteristics of Vestfonna and De Geerfonna (Nordaustlandet, Svalbard) – a spatiotemporal analysis based on multiyear snow-pit data, Geogr. Ann. A, 93, 273-285, doi: 10.1111/j.1468-0459.2011.00440.x, 2011.

Murphy, B. F., Marsiat, I., and Valdes, P.: Atmospheric contributions to the surface mass balance of Greenland in the HadAM3 atmospheric model, J. Geophys. Res.-Atmos., 107, 4556, doi:10.1029/2001JD000389, 2002.

Nakicenovic, N. and Swart, R.: Special Report on Emissions Scenarios, Cambridge University Press, UK, 612 pp., 2000.

Noguer, M., Jones, R., and Murphy, J.: Sources of systematic errors in the climatology of a regional climate model over Europe, Clim. Dynam., 14, 691–712, 1998.

Nordli, ø. and Kohler, J.: The early 20th century warming. Daily observations at Grnfjorden and Longyearbyen on Spitsbergen, Tech. Rep. 12/03, DNMI/klima, 2004.

Nuth, C., Moholdt, G., Kohler, J., Hagen, J. O., and Kb, A.: Svalbard glacier elevation changes and contribution to sea level rise, J. Geophys. Res., 115, F01008, 16 pp., doi:10.1029/2008JF001223, 2010.

Oerlemans, J. and Reichert, B.: Relating glacier mass balance to meteorological data by using a seasonal sensitivity characteristic, J. Glaciol., 46, 1–6, 2000.

Oerlemans, J., Bassford, R. P., Chapman, W., Dowdeswell, J. A., Glazovsky, A. F., Hagen, J. O., Melvold, K., de Wildt, M. D., and van de Wal, R. S. W.: Estimating the contribution of Arctic glaciers to sea-level change in the next 100 years, Ann. Glaciol., 42, 230–236, 2005.

Overland, J. E. and Wang, M.: Future regional Arctic sea ice declines, Geophys. Res. Lett., 34, L17705, 7 pp., doi:10.1029/2007GL030808, 2007.

Pinglot, J. F., Pourchet, M., Lefauconnier, B., Hagen, J. O., Isaksson, E., Vaikmae, R., and Kamiyama, K.: Accumulation in Svalbard glaciers deduced from ice cores with nuclear tests and Chernobyl reference layers, Polar Res., 18, 315–321, 1999.

Polyak, L., Alley, R. B., Andrews, J. T., Brigham-Grette, J., Cronin, T. M., Darby, D. A., Dyke, A. S., Fitzpatrick, J. J., Funder, S., Holland, M., Jennings, A. E., Miller, G. H., O'Regan, M., Savelle, J., Serreze, M., St. John, K., White, J., Wolff, E.: History of sea ice in the Arctic, Quaternary Sci. Rev., 29, 1757–1778, 2010.

Pope, V. D., Gallani, M. L., Rowntree, P. R., and Stratton, R. A.: The impact of new physical parametrizations in the Hadley Centre climate model: HadAM3, Clim. Dynam., 16, 123–146, 2000.

Raper, V., Bamber, J., and Krabill, W.: Interpretation of the anomalous growth of Austfonna, Svalbard, a large Arctic ice cap, Ann. Glaciol., 42, 373–379, 2005.

Rayner, N. A., Parker, D. E., Horton, E. B., Folland, C. K., Alexander, L. V., Rowell, D. P., Kent, E. C., and Kaplan, A.: Global analyses of sea surface temperature, sea ice, and night marine air temperature since the late nineteenth century, J. Geophys. Res.-Atmos., 108, 4407, 29 pp., doi:10.1029/2002JD002670, 2003.

Rinke, A. and Dethloff, K.: Simulated circum-Arctic climate changes by the end of the 21st century, Global Planet. Change, 62, 173–186, 2008.

Rogers, A. N., Bromwich, D. H., Sinclair, E. N., and Cullather, R. I.: The Atmospheric Hydrologic Cycle over the Arctic Basin from Reanalyses. Part II: Interannual Variability, J. Climate, 14, 11, 2414–2429, 2001.

Rye, C. J., Arnold, N. S., Willis, I. C., and Kohler, J.: Modeling the surface mass balance of a high Arctic glacier using the ERA-40 reanalysis, J. Geophys. Res.-Earth, 115, F02014, 18 pp., doi:10.1029/2009JF001364, 2010.

Sand, K., Winther, J. G., Marechal, D., Bruland, O., and Melvold, K.: Regional variations of snow accumulation on Spitsbergen, Svalbard, 1997–99, Nord. Hydrol., 34, 17–32, 2003.

Serreze, M., Holland, M. M., and Stroeve, J.: Perspectives on the Arctic's Shrinking Sea-Ice Cover, Science, 315, 5818, 1533–1536, doi:10.1126/science.1139426, 2007.

Serreze, M. C., Barrett, A. P., Stroeve, J. C., Kindig, D. N., and Holland, M. M.: The emergence of surface-based Arctic amplification, Cryosphere, 3, 11–19, 2009.

Sharp, M. and Wang, L. B.: A Five-Year Record of Summer Melt on Eurasian Arctic Ice Caps, J. Climate, 22, 133–145, 2009.

Singarayer, J. S., Bamber, J. L., and Valdes, P. J.: Twenty-first-century climate impacts from a declining Arctic sea ice cover, J. Climate, 19, 1109–1125, 2006.

Skelly, W. C. and Henderson-Sellers, A.: Grid Box or Grid Point: what type of data do GCMs deliver to Climate Impacts Researchers?, Int. J. Climatol., 16, 1079–1086, 1996.

Stein, U. and Alpert, P.: Factor separation in numerical simulations, J. Atmos. Sci., 50, 2107–2115, 1993.

Stroeve, J., Holland, M. M., Meier, W., Scambos, T., and Serreze, M.: Arctic sea ice decline: Faster than forecast, Geophys. Res. Lett., 34, L09501, doi:10.1029/2007GL029703, 2007.

Taurisano, A., Schuler, T. V., Hagen, J. O., Eiken, T., Loe, E., Melvold, K., and Kohler, J.: The distribution of snow

accumulation across the Austfonna ice cap, Svalbard: direct measurements and modelling, Polar Res., 26, 1, 7–13.

Van de Wal, R. S. W. and Oerlemans, J.: An energy-balance model for the Greenland ice-sheet, Global Planet. Change, 9, 115–131, 1994.

Walczowski, W. and Piechura, J.: Influence of the West Spitsbergen Current on the local climate, Int. J. Climatol., 31, 1097–0088, 2011.

Wang, M. Y. and Overland, J. E.: A sea ice free summer Arctic within 30 years?, Geophys. Res. Lett., 36, L07502, doi:10.1029/2009GL037820, 2009.

Wilson, M. F. and Henderson-Sellers, A.: A global archive of land cover and soils data for use in general circulation climate models, J. Climatol., 5, 119–143, 1985.

Wouters, B., Chambers, D., and Schrama, E. J. O.: GRACE observes small-scale mass loss in Greenland, Geophys. Res. Lett, 35, L20501, doi:10.1029/2008GL034816, 2008.

Yamamoto, K., Tachibana, Y., Honda, M., and Ukita, J.: Intra-seasonal relationship between the Northern Hemisphere sea ice variability and the North Atlantic Oscillation, Geophys. Res. Lett, 33, L14711, doi:10.1029/2006GL026286, 2006.